

Imaging perylene derivatives on rutile TiO₂(110) by noncontact atomic force microscopy

J. Schütte, R. Bechstein, P. Rahe, M. Rohlfing, and A. Kühnle*

Fachbereich Physik, Universität Osnabrück, Barbarastr. 7, 49076 Osnabrück, Germany

H. Langhals

Department Chemie, Ludwig-Maximilians-Universität (LMU) München, Butenandtstr. 13, 81377 München, Germany

(Received 8 October 2008; revised manuscript received 27 November 2008; published 30 January 2009)

The adsorption of 3,4,9,10-perylene tetracarboxylic diimide derivative molecules on the rutile TiO₂(110) surface was investigated by noncontact atomic force microscopy and density-functional theory (DFT) calculations. After submonolayer deposition, individual molecules are observed to adsorb with their main axis aligned along the [001] direction and centered on top of the bridging oxygen rows. Depending on the tip termination, two distinctly different molecular contrasts are achieved. In the first mode, the molecules are imaged as bright elongated features, while in another mode the molecules appear with a bright rim and a dark bow-shaped center. Comparison with the defect density on the bare TiO₂(110) surface suggests that the molecules preferentially anchor to surface defects. Our DFT calculations reveal details of the molecular adsorption position, confirming the experimentally observed adsorption on top of the bridging oxygen rows. The DFT results indicate that diffusion along the rows should be quite easily possible, while diffusion perpendicular to the rows seems to be hindered by a significant energy barrier.

DOI: [10.1103/PhysRevB.79.045428](https://doi.org/10.1103/PhysRevB.79.045428)

PACS number(s): 68.37.Ps, 68.43.Fg, 81.07.-b

I. INTRODUCTION

The adsorption of organic molecular semiconductors onto various substrate surfaces has attracted considerable attention due to the promising applications of these organic molecules in flexible, low-cost, and tailor-made (opto)electronic devices such as light-emitting diodes, transistors, and solar cells.^{1,2} Perylene and its derivatives represent a prominent class of molecular organic semiconductors as these molecules exhibit great flexibility in design.³ Consequently, perylene derivatives became prototype molecules for a vast number of fundamental adsorption and organic thin film growth studies. Besides 3,4,9,10-perylene tetracarboxylic acid-dianhydride (PTCDA), a great number of other perylene derivatives have been studied, including 3,4,9,10-perylene tetracarboxylic diimine (PTCDI).^{4,5} These molecules have been deposited on various conducting surfaces including Ag, Au, Cu, and highly oriented pyrolytic graphite⁶⁻¹⁸ as well as semiconducting¹⁹⁻²² and insulating substrates such as KBr, KCl, NaCl, and mica.²³⁻²⁸ Titanium dioxide plays a prominent role due to its promising properties for a wide range of various applications such as catalysis and solar cells.^{29,30}

Noncontact atomic force microscopy (NC-AFM) has been proven to be a powerful method for atomic-resolution imaging on a broad range of substrates.³¹⁻³³ Using NC-AFM, individual molecules have been resolved in a few instances so far, including, e.g., carboxylic acids on TiO₂(110) (Refs. 34-36) as well as porphyrin derivatives on Au(111) (Ref. 37) and on SrTiO₃(100).³⁸ Unlike in scanning tunneling microscopy (STM), however, understanding contrast formation in NC-AFM imaging is still far from being mature and only few examples exist, revealing further insight into mechanisms behind contrast formation. These instances have been limited to bare substrate surfaces so far.³⁹⁻⁴²

Here we present a combined experimental and theoretical investigation of the adsorption of individual perylene derivative molecules on the (110) surface of rutile TiO₂. High-

resolution NC-AFM imaging reveals two distinctly different molecular contrast modes that can be explained by different tip terminations.

Density-functional theory (DFT) calculations have provided a detailed picture of the TiO₂(110) surface, including a number of prominent surface defects.⁴³⁻⁴⁵ DFT calculations have also revealed details of the adsorption of organic molecules on various substrates, including metals, insulators, and mostly conventional semiconductors. All these investigations show that DFT calculations provide a comprehensive understanding of adsorption processes. DFT studies of adsorption on TiO₂ are quite rare so far.⁴⁶⁻⁴⁹ Here we present DFT studies of PTCDI on TiO₂(110), aiming at clarifying questions regarding the precise adsorption position on the surface and diffusion processes of the molecule along the surface.

II. METHODS

Experiments were performed in an ultrahigh vacuum (UHV) system with a base pressure usually lower than 1×10^{-10} mbar. The system is equipped with a VT AFM 25 atomic force microscope (Omicron, Taunusstein, Germany) and an easy PLL plus phase-locked loop controller and detector (Nanosurf, Liestal, Switzerland) for oscillation excitation and signal demodulation. For NC-AFM measurements we used *n*-doped silicon cantilevers (NanoWorld, Neuchâtel, Switzerland) with a resonance frequency of about 300 kHz (type PPP-NCH) operated at an amplitude of about 10 nm. Prior to use, the cantilevers were Ar⁺ sputtered at 2 keV for 5 min to remove contaminants. For all images shown here, the distance feedback loop was set very slow in order to provide quasiconstant-height images while still following the overall tilt of the sample surface. All images were taken with a scanning speed of 1 line per second and 500 pixel per line. Fast and slow scan directions are given by the arrows in the

upper right corner in each image. The images are displayed such that bright areas correspond to high attractive interaction while dark corresponds to less attractive or even repulsive interactions.⁵⁰ For STM measurements we used tungsten tips manufactured by Omicron.

The molecule used in this study is a PTCDI derivative, namely, *N,N'*-bis(1-hexylheptyl)-PTCDI.⁵¹ The chemical structure of this molecule, referred to as PTCDI S-13, is displayed in Fig. 1(a). We performed few experiments with PTCDI molecules without alkyl chain functionalization, resulting in qualitatively similar results. As the majority of the data were taken with PTCDI S-13, only these results are presented here. The S-13 molecules were outgassed at 400 K for 12 h before deposition and sublimated *in situ* from a home-made Knudsen cell heated to 455 K. The submonolayer coverages shown here were obtained after 5 min sublimation onto the sample held at room temperature positioned ~ 9 cm apart from the Knudsen cell.

PTCDI S-13 was studied on the rutile titanium dioxide (110) surface. A model of this surface is shown in Fig. 1(b). The TiO_2 samples are crystals of highest available quality (MTI, Richmond, USA). The unreconstructed (110) surface was prepared by repeated cycles of Ar^+ sputtering at 1 kV for 15 min and annealing at 990 K for 15 min. After cleaning, the surface was examined thoroughly by both STM and NC-AFM, obtaining atomic resolution for evaluating the surface cleanliness and the density of surface defects.

Several different contrast modes are known for NC-AFM images of the bare titanium dioxide surface. Two of them have been ascribed to positive and negative tip terminations, respectively.⁴⁰ With a negatively (positively) terminated tip, the titanium rows are imaged bright (dark), while the bridging oxygen rows are imaged dark (bright). These two modes can be distinguished by the position of the defects in the bridging oxygen rows [vacancies, single hydroxyls, and double hydroxyls; see Figs. 1(b)]. For a negatively terminated tip the defects appear as bright features in the dark oxygen row, while they are imaged as dark depressions in the bright oxygen row for a positively terminated tip. Besides these two contrast modes, yet another contrast mode has been reported in literature that cannot be explained by the simple picture of pure electrostatic interactions.⁵²

III. EXPERIMENTAL RESULTS

Figure 1(c) shows an NC-AFM quasiconstant-height image of the molecule-covered $\text{TiO}_2(110)$ surface after 5 min sublimation at 455 K. In this overview, the surface topography of the $\text{TiO}_2(110)$ surface is shown with flat areas having a typical size of about 40×40 nm². The molecules appear as bright elongated features. Besides very few exceptions, the main axis of the molecules is aligned along the [001] direction. This alignment is further confirmed by the high-resolution images shown in Figs. 2 and 3. The molecules do not cluster at step edges but are homogeneously distributed over the surface. Annealing the substrate at temperatures up to 500 K does not change the overall picture of individual molecules scattered over the surface. Analyzing the size of the molecular features in small-scale images allows us to

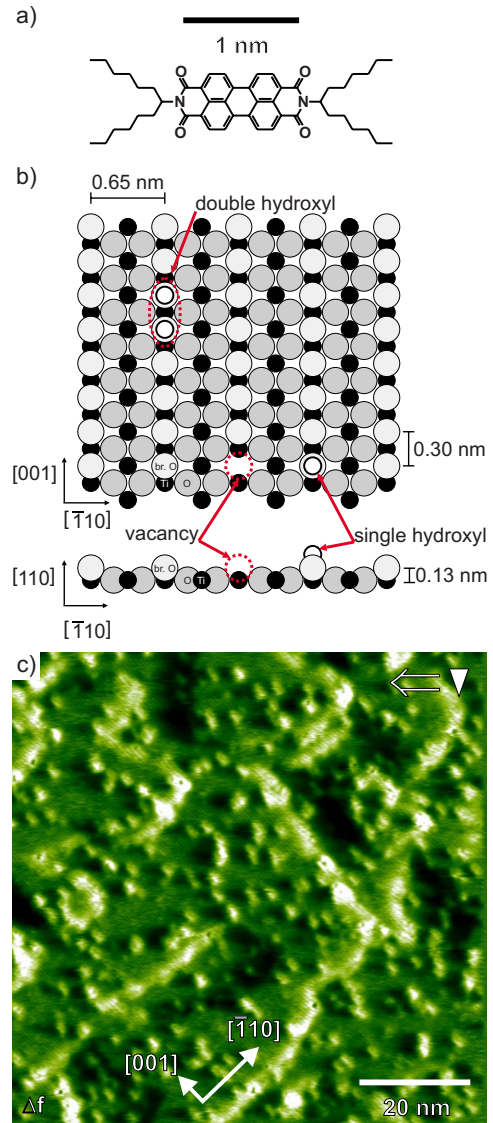


FIG. 1. (Color online) (a) Schematic drawing of an *N,N'*-bis(1-hexylheptyl)-PTCDI (PTCDI S-13) molecule (CAS No. 110590-84-6). (b) Schematic drawing of the bulk-truncated rutile $\text{TiO}_2(110)$ surface with bridging oxygen rows along the [001] direction. Titanium atoms are shown in small black circles. Oxygen atoms are shown in gray circles; lighter shading represents higher atoms. Defects in the bridging oxygen row are marked by arrows, showing an oxygen vacancy as well as single and double hydroxyls. (c) Quasiconstant-height NC-AFM image (average detuning $\Delta f = -10$ Hz) of the rutile $\text{TiO}_2(110)$ surface after 5 min sublimation of PTCDI S-13. Homogeneously distributed molecules are observed, aligned with their main axis along the [001] direction. The $\text{TiO}_2(110)$ sample was subjected to 22 cycles of sputtering and annealing in total.

determine the typical width of about 1.0 ± 0.1 nm and length of about 2.6 ± 0.2 nm.

A high-resolution image of a molecule-covered terrace is shown in Fig. 2. In this imaging mode (mode I), individual molecules can be identified as bright features aligned with their main axis along the [001] direction. The close-packed rows of the titanium dioxide substrate appear as bright and

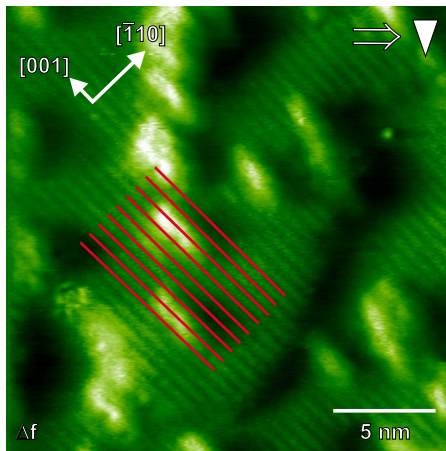


FIG. 2. (Color online) Quasiconstant-height NC-AFM image (average detuning $\Delta f = -6$ Hz) of PTCDI S-13 molecules on a rutile $\text{TiO}_2(110)$ terrace. In this imaging mode (mode I), the molecules appear as bright elongated features. The main axis of which is aligned along the $[001]$ direction of the substrate. Lines are superimposed onto the dark rows of the substrate, illustrating that the molecules are centered on the dark rows. The $\text{TiO}_2(110)$ sample was subjected to 24 cycles of sputtering and annealing in total.

dark lines running along the $[001]$ direction. The $\text{TiO}_2(110)$ sample shown here was subjected to 24 cycles of sputtering and annealing. Note that no defects are seen on the bare terrace beside the molecules in this figure, although surface defects are known to be present after 24 cycles of sputtering and annealing.⁵³ This finding indicates that the molecules anchor to surface defects. To clarify the adsorption position of the molecules with respect to the $[\bar{1}10]$ direction in mode I, we have superimposed lines to the dark substrate rows, illustrating that the molecules are centered on the *dark* substrate rows.

Besides the imaging contrast presented in Figs. 1 and 2, we occasionally observe another contrast. This is obtained after tip changes such as a tip-surface contact at which the tip might pick up species from the surface or drop material onto the surface. In this second imaging mode (mode II), the molecules exhibit a dark center surrounded by a bright rim, as shown in Fig. 3. The dark inner region appears as a bow-like structure which is branched at both ends. The bending of the bowlike structure is independent of the scan direction [compare Figs. 3(a) and 3(b)], indicating that the bending represents a true molecular feature and not only an imaging artifact. The apparent size of the molecules imaged in mode II correspond to the PTCDI core, i.e., the alkyl chains are not imaged. A statistical analysis reveals 169 ± 5 molecules with bending to the right and 153 ± 5 molecules with bending to the left, corresponding to a $(52 \pm 2)\% - (48 \pm 2)\%$ -distribution. As in the previous image in Fig. 2, no defects are seen in Fig. 3, again indicating that the molecules anchor to the defects. In Fig. 3(a) we have superimposed lines to the dark substrate rows. As can be seen from this image, in imaging mode II the molecules are centered on the *bright* substrate rows.

In total we have collected a number of 85 images revealing individual molecules in a series of seven sessions. Out of

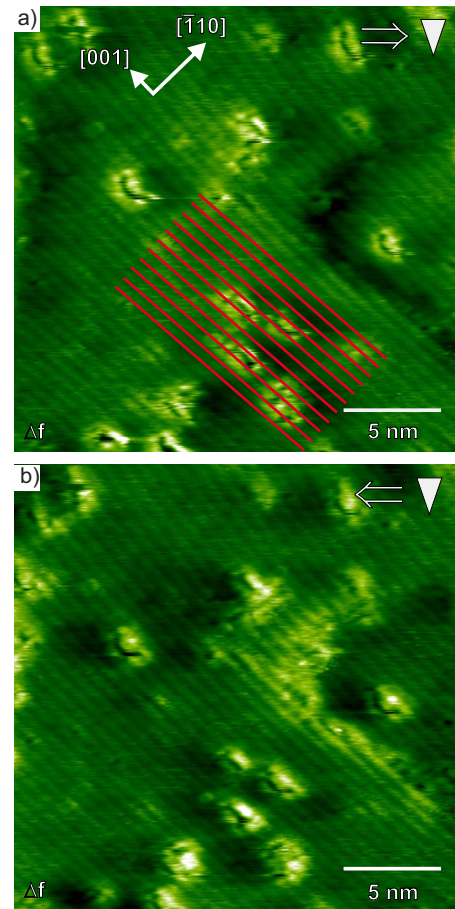


FIG. 3. (Color online) (a) Quasiconstant-height NC-AFM image (average detuning $\Delta f = -6$ Hz) of PTCDI S-13 molecules on a rutile $\text{TiO}_2(110)$ terrace. In this imaging mode (mode II), the molecules exhibit a dark center and a bright rim. Lines are superimposed onto the dark rows of the substrate, illustrating that the molecules are centered on the bright rows. The dark center appears as bowlike structure, which is branched at both ends. The bending is independent of the scan direction. This can be seen by comparison with (b), which is the corresponding backward scan to (a). The $\text{TiO}_2(110)$ sample was subjected to 20 cycles of sputtering and annealing in total.

these images, 52 images reveal mode I, while 33 images exhibit mode II.

In order to clarify the adsorption position of the molecules with respect to the $[\bar{1}10]$ direction, we have performed STM measurements. Using STM, usually the unoccupied states of the fivefold coordinated Ti atoms in the troughs dominate the tunneling current, resulting in a bright appearance of the Ti rows in STM.⁵⁴ In Fig. 4 we present a quasiconstant-current STM image of a molecule-covered terrace. The molecules appear as bright features similar to the structures observed in mode I in NC-AFM. Superimposing lines to the dark rows of this image reveals that the molecules are centered on the dark rows when imaged with STM. Thus, we conclude from our STM results that the molecules adsorb centered on the bridging oxygen rows.

Based on our STM results we can ascribe the observed contrast in both imaging modes. In imaging mode I the mol-

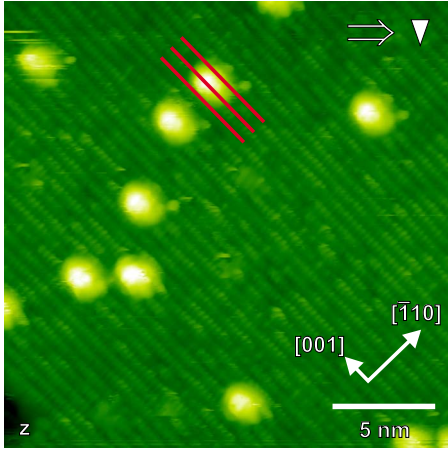


FIG. 4. (Color online) Quasiconstant-current STM z image ($I_t = 0.01$ nA and $U_{\text{bias}} = -1.9$ V are applied to the tip) of PTCDI S-13 on a rutile $\text{TiO}_2(110)$ terrace. The molecules appear as bright features. Lines are superimposed onto the dark rows of the substrate, illustrating that the molecules are centered on the dark, i.e., oxygen rows. The $\text{TiO}_2(110)$ sample was subjected to 24 cycles of sputtering and annealing in total.

olecules are centered on dark rows, i.e., the oxygen rows are imaged dark while the titanium rows are imaged bright. On the other hand, in mode II the molecules are centered on bright rows, i.e., the oxygen rows are imaged bright in this mode. Comparing these results with the NC-AFM imaging contrast published in literature⁴⁰ we might assign the observed contrast modes I and II to negative and positive tip terminations, respectively. We want, however, to stress that the rather simple picture of purely electrostatic interactions might be insufficient to account for all possible interactions mechanisms between the NC-AFM tip and the titanium dioxide surface.

To confirm the above drawn conclusion that the molecules anchor to the defect sites, we studied the defects in more detail. The number of surface defects is known to depend on the surface cleaning procedure.⁵³ Upon sputtering and annealing, surface oxygen vacancies are formed in the bridging oxygen rows. Subsequently, these oxygen vacancies react with water from the residual background gas to form double hydroxyls, which dissociate to eventually form single hydroxyls, i.e., one oxygen vacancy results in two single hydroxyls. In our experiments, we predominantly observe only one type of defect species. The density of these defects does not change even after keeping the sample up to 4 days in the microscope without further cleaning cycles, suggesting these defects to be single hydroxyls. Only occasionally, three different types of defects are observed simultaneously (not shown). In this case, one defect type is ascribed to oxygen vacancies, while the other two are single and double hydroxyls. In Fig. 5 we plot the density of hydroxyls against the so-called “sample history” that has been defined as product of annealing time and annealing temperature.⁵³ For this figure, we have multiplied the numbers of both oxygen vacancies and double hydroxyls by a factor of 2 before adding these numbers to the number of single hydroxyls in order to compare samples with only one type of defect with those

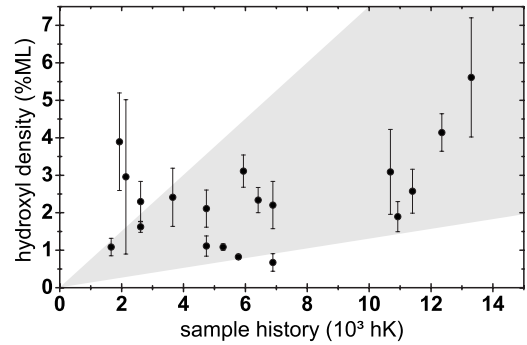


FIG. 5. Hydroxyl density as a function of sample history. The percentage of monolayer single hydroxyls is shown (1 ML corresponds to one hydroxyl per unit cell) against the product of annealing time and annealing temperature. Note that also images with three different types of defects have been included in this graph; the numbers of both oxygen vacancies and double hydroxyls have been multiplied by a factor of 2 before adding to the number of single hydroxyls, as one oxygen vacancy transforms into two single hydroxyl defects. The data shown here are obtained from NC-AFM images solely and were collected from five different samples. Differences in hydroxyl densities for a given sample history are ascribed to slight differences in sample handling (e.g., mounting, preparation, and temperature readout), having a substantial effect on the sample history. Although a rather broad variation in hydroxyl density is observed, an overall trend of increasing hydroxyl density upon increasing sample history can be seen, illustrated by the gray area corresponding to typically observed hydroxyl densities.

exhibiting three types of defects. As can be seen, the defect density is on the order of 1%–5% monolayer (ML) for sample histories in the range of 2–8 kKh, while an increase in hydroxyl density can be seen for higher sample histories. Compared with the data presented in Ref. 53, the densities measured in our experiments are smaller by a factor of ~ 2 . This can be easily explained by different sputtering and annealing parameters (e.g., shorter sputtering and annealing times) and specific sample mounting and heating-ramp conditions that very likely have nonlinear influence on the defect density.

A number of 20–24 cleaning cycles corresponds to a sample history of 5–6 kKh. According to Fig. 5, the defect density is roughly on the order of $(3 \pm 2)\%$ ML for such a sample. This density is large enough to observe hydroxyl defects on a bare surface with NC-AFM. The fact that no defects are seen in Figs. 1–4, therefore, strongly suggests that the molecules anchor to the surface defects. It is interesting that not a single defect is seen in this case, as a sublimation time of 5 min results in a molecule density of $(1.10 \pm 0.46)\%$ ML,⁵⁵ suggesting very few free defects to exist beside the molecules. NC-AFM is, however, a very local technique and the sampled area is rather small, explaining why no defects were observed in our images.

We have increased the number of defects by increasing the number of cleaning cycles to 40, corresponding to an increase in sample history to ~ 10 kKh. In this case, the defect density should be higher than the molecule density of around 1% ML after 5 min sublimation. In Fig. 6(a), an overview over several molecule-covered terraces is shown

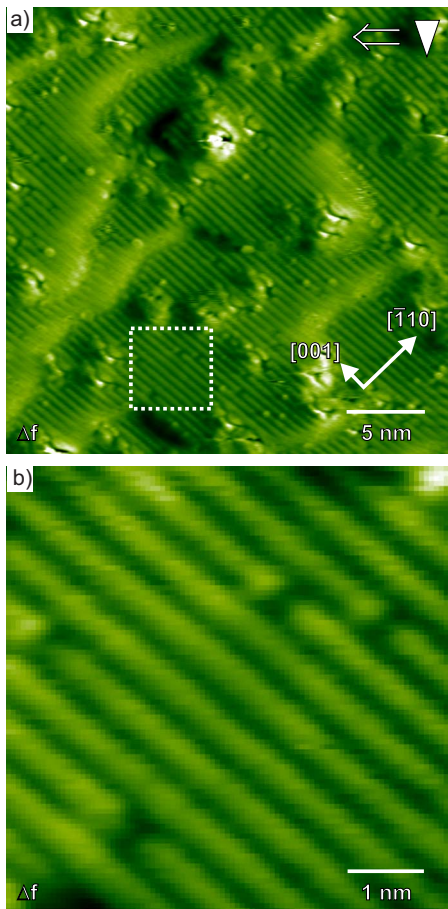


FIG. 6. (Color online) (a) Quasiconstant-height NC-AFM image (average detuning $\Delta f = -7$ Hz) of PTCDI S-13 molecules on a rutile $\text{TiO}_2(110)$ terrace. The molecules are imaged in mode II. The $\text{TiO}_2(110)$ sample was subjected to 40 cycles of sputtering and annealing in total. Defects are seen on the bare terrace besides the molecules. Note that two types of defects (dark and bright) are seen in this case (see text). (b) Zoom into the marked area in (a), revealing atomically resolved bright rows with dark defects, indicates that the bridging oxygen rows are imaged bright.

after 40 cleaning cycles and subsequent molecule sublimation for 5 min, revealing the close-packed rows of the substrate and individual molecules that are imaged in mode II. Besides the molecules, defects are, indeed, visible, as can be seen in Fig. 6(b), showing a zoom into the marked area of Fig. 6(a). These defects are imaged on the bright rows, i.e., the oxygen rows are imaged bright in this case, in agreement with the assignment made before.

IV. THEORETICAL RESULTS

To elucidate the detailed adsorption position of PTCDI on the rutile (110) surface we have performed DFT calculations. We employ the SIESTA package,⁵⁶ using *ab initio* pseudopotentials and the local-density approximation (LDA) which often describes adsorption phenomena more precisely than the generalized gradient approximation (GGA).¹⁰ A double-zeta plus polarization (DZP) basis set with rather delocalized atomic orbitals (extent up to 3.6 Å, corresponding to a very

small contraction energy shift of 0.002 Ry in the preparation of the orbitals⁵⁶) accounts for subtle long-ranged electronic-structure details in the interaction between substrate and adsorbate. The Ti semicore states (*3s* and *3p*) are fully included as valence states, i.e., the pseudopotential core corresponds to a Ti^{12+} ion.

Our TiO_2 rutile lattice constants amount to 4.55 and 2.95 Å compared to measured values of 4.59 and 2.96 Å accompanied by an internal parameter of $u=0.30$ compared to the experimental value of 0.31 (for a definition of the internal parameter see, e.g., Ref. 57). On the (110) surface we observe slight vertical relaxation of the bridging oxygen atoms by 0.13 Å and of the Ti atoms underneath by 0.29 Å toward the vacuum. The Ti atoms in the troughs, on the other hand, relax inward by 0.14 Å. The entire surface thus undergoes moderate distortion as a consequence of broken chemical bonds.^{43,44,58,59} These distortions are significantly stronger than found in ionic oxides but not as strong as found in conventional group-IV or group-III-V semiconductor.

The adsorption of PTCDI on rutile (110) constitutes a big challenge to DFT. In order to arrive at meaningful data, we employ two simplifications. On one hand, we focus on bare PTCDI without the alkyl chain side groups, which are known to be of secondary importance for the adsorption process. The adsorption of this molecule can be described within a 2×6 lateral supercell of TiO_2 without significant interaction of the molecule with its periodic replica. On the other hand, the experimental observation that the molecule and the substrate remain rather unchanged by the adsorption motivates us to investigate the process without full geometry optimization. Instead, we confine the substrate and the molecule in their own geometries [i.e., free rutile (110) surface as described above and gas-phase PTCDI] and simply move the rigid molecule relative to the surface. Based on the experimental findings, we can constrain the theoretical calculations to a molecule that is oriented along the [001] direction.

The adsorption structure is thus described by four parameters only, i.e., the lateral position X of the PTCDI center perpendicular to the surface rows, its lateral position Y along the rows in [001] direction, its height Z above the surface, and the tilt angle Φ of the PTCDI molecule around its long axis. We sample this four-dimensional configurational space with a grid of $\Delta X = 0.65$ Å, $\Delta Y = 0.73$ Å, $\Delta Z = 0.32$ Å, and $\Delta \Phi = 10^\circ$. For each configuration the DFT total energy of the system is calculated. Thereafter the energy is optimized with respect to the parameters by polynomial approximation and least-squares fitting. While this procedure (i.e., the neglect of structural deformation of substrate and molecule upon adsorption) may not be accurate enough to draw final conclusions on precise adsorption energies and details of the adsorption geometry, it allows us to focus on adsorption sites and orientations from a more general point of view. Full geometry optimization has been shown to be extremely slow and, for a system of such complex nature as the present one, might be subjected to being trapped in side minima, leading to wrong conclusions concerning the adsorption site.

Several characteristic geometries obtained from our DFT data are shown in Fig. 7 as a cross section through substrate and molecule, with the line of vision along the long axis of the molecule. Further details are given in Table I. The lower

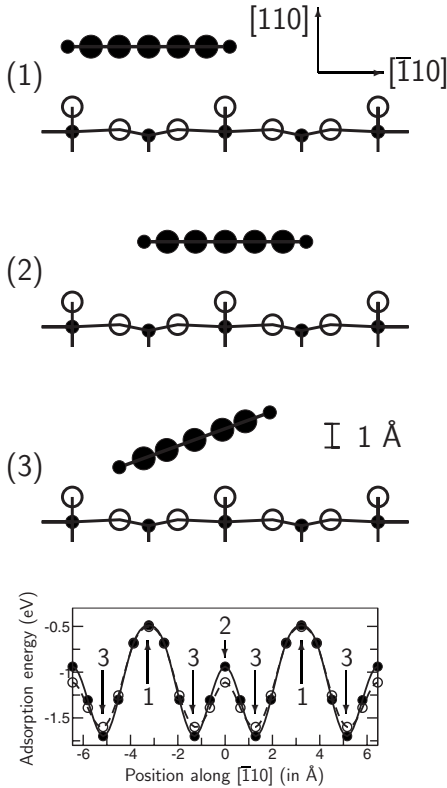


FIG. 7. Calculated adsorption structures of PTCDI on the rutile (110) surface. The three upper panels show a cross section of the surface, with the line of vision along the surface rows which is also the long axis of the molecule (cf. Fig. 1). The molecule is shown with five carbon atoms of the core cross section plus two hydrogen atoms at each side. Configuration (3) is the optimal adsorption configuration. The lower panel shows the corresponding adsorption energies (see text) in dependence of the position of the molecule center along the $[\bar{1}10]$ direction.

panel of Fig. 7 shows the resulting adsorption energies as a function of X , i.e., as a function of the lateral position of the center of the molecule perpendicular to the surface rows. The parameters Z and Φ (height and tilt angle) have already been optimized by a minimization procedure, leading (among others) to the structures shown in the upper panels. The filled and open circles in the lower panel indicate the data calculated for the parameter X from the grid, while the solid and

TABLE I. Calculated height of the center of the molecule relative to the bridging oxygen atoms, tilting angle (relative to flat-lying orientation), and adsorption energy for three characteristic configurations: (1) molecular axis above the Ti trough atoms, (2) molecular axis above the bridging oxygen atoms, and (3) optimized configuration. The last column shows the diffusion barrier for diffusion in the direction of the rows.

Configuration	Height (Å)	Tilt angle (deg)	E_{ads} (eV)	E_{diff} (eV)
(1) above Ti	2.53	0	-0.5	~0.0
(2) above O	2.56	0	-0.9	~0.2
(3) optimized	2.51	22	-1.7	~0.1

dashed curves show spline fits to the data. Two sets of data are shown. The solid line and filled circles refer to the Y value of the PTCDI center coinciding with a Ti trough atom. The dashed line and open circles, on the other hand, refer to the Y value coinciding with a bridging O atom. In the case of structure (2), e.g., the open circle refers to the PTCDI center directly above a bridging O atom while the filled circle refers to the PTCDI center between two adjacent O atoms.

Two high-symmetry configurations (1) and (2) deserve particular attention. In configuration (1) the center of the molecule is located above the Ti atoms in the trough. In this configuration some binding occurs between the bridging oxygen atoms and the hydrogen atoms of the molecule. The distance to the Ti trough atoms amounts to 3.7 Å, which is too large to contribute significantly to the binding. Closer distance to the Ti atoms is not possible since it would lead to steric hindrance between the hydrogen atoms of the PTCDI molecule and oxygen atoms of the surface. This configuration has a binding energy of about 0.5 eV only, thus constituting the least favorable adsorption site. In configuration (2), on the other hand, the center of the molecule is located above an oxygen row, which leads to stronger binding than in configuration (1). The adsorption energy varies between 0.9 and 1.1 eV depending on the Y position of the molecular center. The stronger binding energy is found when the PTCDI center is exactly on top of a bridging O atom (open circle in the lower panel of Fig. 7).

The most favorable adsorption site, however, is achieved when the molecule “slides down” into the trough, thus keeping the bond to the bridging oxygen atoms and simultaneously increasing the interaction with the trough. This lateral movement by 1.3 Å is accompanied by a tilting of 22° and gains about 0.7 eV in adsorption energy. Note that sliding and tilting into the other direction are equally possible.

From all these data we observe that PTCDI adsorbs on the bridging oxygen rows, as had already been concluded from the NC-AFM data. However, the adsorption site is not exactly on top of the row but is shifted to the side by about 1.3 Å. The molecule is significantly closer to the surface at this side, while its other side sticks out into the vacuum [see panel (3) in Fig. 7]. This means that the lateral displacement might be difficult to detect in NC-AFM since the part of the molecule which sticks out would give a stronger signal. If an experiment managed to show the asymmetry of the adsorption, it should observe two possible configurations [i.e., configuration (3) and its counterpart with sliding and tilting in the opposite direction], which are separated from each other by an energy barrier of about 0.7 eV [i.e., the adsorption-energy difference between configurations (2) and (3)].

In all configurations a significant adsorption energy is observed. This indicates that strong binding is achieved regardless of geometrical details, making desorption unlikely. The difference in adsorption energy of 1.2 eV between the optimal and the least favorable adsorption sites strongly inhibits diffusion perpendicular to the rows. Diffusion *along* the rows, on the other hand, is facilitated by the relatively small variance of the adsorption energy for movement in this direction. This variance, i.e., the diffusion barrier, is given by the difference between the two curves in the lower panel of Fig. 7. Here we find a variance of only about 0.1 eV for the

optimized configuration (3) when the molecule is moved along the rows. However, these data should not be taken too literally since the current approximations (rigid molecule and substrate) and available DFT functionals do not allow giving the adsorption energies with the accuracy necessary to draw final conclusions concerning such small energy differences. Nonetheless, our calculations do confirm the experimental finding that diffusion should be easily possible along the rows, thus allowing each molecule to find an anchoring defect site. Note, however, that alkyl side chains attached to the molecule, as often included in experiments, might change the diffusion behavior significantly.

V. SUMMARY AND CONCLUSION

To summarize, we have observed individual PTCDI derivative molecules with NC-AFM, revealing submolecular resolution within the molecules. Two distinctly different molecular contrast modes were observed, revealing the molecules either bright and unstructured (mode I) or as features with dark center and bright rim (mode II). The change in the observed contrast modes coincides with a change in the contrast of the titanium dioxide substrates. We can unambiguously determine the adsorption position of the molecules along the $[\bar{1}10]$ direction from both our DFT calculations and the comparison with STM experiments, revealing that

the molecules adsorb on the bridging oxygen rows. Our DFT calculations show, however, that the molecules are not located exactly on top of the oxygen rows but are slightly displaced toward the Ti troughs, gaining about 0.7 eV in binding energy. Since the molecules are also tilted, the lateral shift is difficult to observe experimentally. Comparing our results with the findings of NC-AFM contrast formation on $\text{TiO}_2(110)$ published in literature,⁴⁰ we might assign the observed contrast modes to negative (mode I) and positive (mode II) tip terminations. However, the tip sample interaction might be much more complicated than suggested by the simple picture of purely electrostatic interaction, calling for more elaborate models for describing the tip-sample interaction. Our experimental results strongly indicate that the molecules anchor to the hydroxyl defects of the titanium dioxide substrate as no defects were seen beside the molecules even after 24 cycles of sputtering and annealing, where a typical defect density of about 3% ML is expected.

ACKNOWLEDGMENTS

This work was supported by the German Research Foundation (DFG) through the Emmy Noether program and the Niedersachsen PhD program "Synthesis and Characterization of Surfaces and Interfaces assembled from Clusters and Molecules."

*kuehnle@uos.de

- ¹S. R. Forrest, *Nature (London)* **428**, 911 (2004).
- ²M. Grätzel, *Nature (London)* **414**, 338 (2001).
- ³S. R. Forrest, *Chem. Rev. (Washington, D.C.)* **97**, 1793 (1997).
- ⁴H. Langhals, *Heterocycles* **40**, 477 (1995).
- ⁵H. Langhals and J. Gold, *Helv. Chim. Acta* **88**, 2832 (2005).
- ⁶V. Shklover, F. S. Tautz, R. Scholz, S. Sloboshanin, M. Sokolowski, J. A. Schaefer, and E. Umbach, *Surf. Sci.* **454-456**, 60 (2000).
- ⁷C. Seidel, A. H. Schäfer, and H. Fuchs, *Surf. Sci.* **459**, 310 (2000).
- ⁸A. Hauschild, K. Karki, B. C. C. Cowie, M. Rohlfing, F. S. Tautz, and M. Sokolowski, *Phys. Rev. Lett.* **94**, 036106 (2005).
- ⁹M. Eremtchenko, J. A. Schaefer, and F. S. Tautz, *Nature (London)* **425**, 602 (2003).
- ¹⁰M. Rohlfing, R. Temirov, and F. S. Tautz, *Phys. Rev. B* **76**, 115421 (2007).
- ¹¹F. S. Tautz, M. Eremtchenko, J. A. Schaefer, M. Sokolowski, V. Shklover, and E. Umbach, *Phys. Rev. B* **65**, 125405 (2002).
- ¹²M. Schneider, E. Umbach, and M. Sokolowski, *Chem. Phys.* **325**, 185 (2006).
- ¹³S. K. M. Henze, O. Bauer, T. L. Lee, M. Sokolowski, and F. S. Tautz, *Surf. Sci.* **601**, 1566 (2007).
- ¹⁴S. Mannsfeld, M. Toerker, T. Schmitz-Hübsch, F. Sellam, T. Fritz, and K. Leo, *Org. Electron.* **2**, 121 (2001).
- ¹⁵M. Stöhr, M. Gabriel, and R. Möller, *Surf. Sci.* **507-510**, 330 (2002).
- ¹⁶S. C. B. Mannsfeld and T. Fritz, *Phys. Rev. B* **69**, 075416 (2004).
- ¹⁷H. Yamane, S. Kera, K. K. Okudaira, D. Yoshimura, K. Seki, and N. Ueno, *Phys. Rev. B* **68**, 033102 (2003).
- ¹⁸F. S. Tautz, *Prog. Surf. Sci.* **82**, 479 (2007).
- ¹⁹J. J. Kolodziej, M. Goryl, J. Konior, F. Krok, and M. Szymonski, *Nanotechnology* **18**, 135302 (2007).
- ²⁰G. Sazaki, T. Fujino, J. T. Sadowski, N. Usami, T. Ujihara, K. Fujiwara, Y. Takahashi, E. Matsubara, T. Sakurai, and K. Nakajima, *J. Cryst. Growth* **262**, 196 (2004).
- ²¹M. Friedrich *et al.*, *J. Phys.: Condens. Matter* **15**, S2699 (2003).
- ²²T. U. Kampen, G. Salvan, D. Tenne, R. Scholz, and D. R. T. Zahn, *Appl. Surf. Sci.* **175-176**, 326 (2001).
- ²³T. Dienel, C. Loppacher, S. C. B. Mannsfeld, R. Forker, and T. Fritz, *Adv. Mater. (Weinheim, Ger.)* **20**, 959 (2008).
- ²⁴T. Kunstmann, A. Schlarb, M. Fendrich, Th. Wagner, R. Möller, and R. Hoffmann, *Phys. Rev. B* **71**, 121403(R) (2005).
- ²⁵H. Proehl, T. Dienel, R. Nitsche, and T. Fritz, *Phys. Rev. Lett.* **93**, 097403 (2004).
- ²⁶H. Proehl, R. Nitsche, T. Dienel, K. Leo, and T. Fritz, *Phys. Rev. B* **71**, 165207 (2005).
- ²⁷L. Nony, R. Bennewitz, O. Pfeiffer, E. Gnecco, A. Baratoff, E. Meyer, T. Eguchi, A. Gourdon, and C. Joachim, *Nanotechnology* **15**, S91 (2004).
- ²⁸D. Schlettwein, A. Back, B. Schilling, T. Fritz, and N. R. Armstrong, *Chem. Mater.* **10**, 601 (1998).
- ²⁹U. Diebold, *Surf. Sci. Rep.* **48**, 53 (2003).
- ³⁰B. O'Regan and M. Grätzel, *Nature (London)* **353**, 737 (1991).
- ³¹F. J. Giessibl, *Science* **267**, 68 (1995).
- ³²M. Reichling and C. Barth, *Phys. Rev. Lett.* **83**, 768 (1999).
- ³³S. Orisaka, T. Minobe, T. Uchihashi, Y. Sugawara, and S.

- Morita, *Appl. Surf. Sci.* **140**, 243 (1999).
- ³⁴K.-I. Fukui, H. Onishi, and Y. Iwasawa, *Chem. Phys. Lett.* **280**, 296 (1997).
- ³⁵A. Sasahara, H. Uetsuka, T. A. Ishibashi, and H. Onishi, *Appl. Surf. Sci.* **188**, 265 (2002).
- ³⁶H. Onishi, A. Sasahara, H. Uetsuka, and T. A. Ishibashi, *Appl. Surf. Sci.* **188**, 257 (2002).
- ³⁷S. Tanaka, H. Suzuki, T. Kamikado, and S. Mashiko, *Thin Solid Films* **438-439**, 56 (2003).
- ³⁸S. Tanaka, H. Suzuki, M. Inada, T. Kamikado, and S. Mashiko, *Nanotechnology* **16**, S107 (2005).
- ³⁹C. Barth, A. S. Foster, M. Reichling, and A. L. Shluger, *J. Phys.: Condens. Matter* **13**, 2061 (2001).
- ⁴⁰J. V. Lauritsen, A. S. Foster, G. H. Olesen, M. C. Christensen, A. Kühnle, S. Helveg, J. R. Rostrup-Nielsen, B. S. Clausen, M. Reichling, and F. Besenbacher, *Nanotechnology* **17**, 3436 (2006).
- ⁴¹A. I. Livshits, A. L. Shluger, A. L. Rohl, and A. S. Foster, *Phys. Rev. B* **59**, 2436 (1999).
- ⁴²A. S. Foster, W. A. Hofer, and A. L. Shluger, *Curr. Opin. Solid State Mater. Sci.* **5**, 427 (2001).
- ⁴³S. J. Thompson and S. P. Lewis, *Phys. Rev. B* **73**, 073403 (2006).
- ⁴⁴G. von Oertzen and A. Gerson, *Int. J. Quantum Chem.* **106**, 2054 (2006).
- ⁴⁵G. Teobaldi, W. A. Hofer, O. Bikondoa, C. Pang, G. Cabailh, and G. Thornton, *Chem. Phys. Lett.* **437**, 73 (2007).
- ⁴⁶M. Rasmussen, L. Molina, and B. Hammer, *J. Chem. Phys.* **120**, 988 (2004).
- ⁴⁷A. V. Bandura, D. G. Sykes, V. Shapovalov, T. N. Troung, J. D. Kubicki, and R. A. Evarestov, *J. Phys. Chem. B* **108**, 7844 (2004).
- ⁴⁸M. L. Sushko, A. Yu. Gal, and A. L. Shluger, *J. Phys. Chem. B* **110**, 4853 (2006).
- ⁴⁹Z.-W. Qu and G.-J. Kroes, *J. Phys. Chem. B* **110**, 23306 (2006).
- ⁵⁰P. Rahe, R. Bechstein, J. Schütte, F. Ostendorf, and A. Kühnle, *Phys. Rev. B* **77**, 195410 (2008).
- ⁵¹S. Demmig and H. Langhals, *Chem. Ber.* **121**, 225 (1988).
- ⁵²G. H. Enevoldsen, A. S. Foster, M. C. Christensen, J. V. Lauritsen, and F. Besenbacher, *Phys. Rev. B* **76**, 205415 (2007).
- ⁵³S. Wendt *et al.*, *Surf. Sci.* **598**, 226 (2005).
- ⁵⁴U. Diebold, J. F. Anderson, K.-O. Ng, and D. Vanderbilt, *Phys. Rev. Lett.* **77**, 1322 (1996).
- ⁵⁵This density is evaluated from 11 drift-free images; the error includes both fluctuations in sublimation as well as statistical deviation due to NC-AFM sampling.
- ⁵⁶J. M. Soler, E. Artacho, J. D. Gale, A. García, J. Junquera, P. Ordejon, and D. Sanchez-Portal, *J. Phys.: Condens. Matter* **14**, 2745 (2002).
- ⁵⁷K. M. Glassford and J. R. Chelikowsky, *Phys. Rev. B* **46**, 1284 (1992).
- ⁵⁸R. Lindsay, A. Wander, A. Ernst, B. Montanari, G. Thornton, and N. M. Harrison, *Phys. Rev. Lett.* **94**, 246102 (2005).
- ⁵⁹H. Perron, J. Vandenborre, C. Domain, R. Drot, J. Roques, E. Simoni, J.-J. Ehrhardt, and H. Catalette, *Surf. Sci.* **601**, 518 (2007).